Solid–liquid interfacial energy of the solid Mg_2Zn_{11} phase in equilibrium with Zn–Mg eutectic liquid

2007 J. Phys.: Condens. Matter 19 176003

(http://iopscience.iop.org/0953-8984/19/17/176003)

J. Phys.: Condens. Matter **19** (2007) 176003 (14pp) doi:10.1088/0953-8984/19/17/176003

Solid–liquid interfacial energy of the solid Mg_2Zn_{11} phase in equilibrium with Zn–Mg eutectic liquid

M Erol[1], K Keşlioğlu[2] and N Maraşlı[2,3]

[1] Department of Physics, Faculty of Arts and Sciences, Bozok University, 66100 Yozgat, Turkey
[2] Department of Physics, Faculty of Arts and Sciences, Erciyes University, 38039 Kayseri, Turkey

E-mail: marasli@erciyes.edu.tr

Received 15 November 2006, in final form 10 March 2007
Published 3 April 2007
Online at stacks.iop.org/JPhysCM/19/176003

Abstract

The Gibbs–Thomson coefficient and solid–liquid interfacial energy of the solid Mg_2Zn_{11} phase in equilibrium with Zn–Mg eutectic liquid have been determined to be $(3.3 \pm 0.2) \times 10^{-8}$ K m and $(20.8 \pm 2.1) \times 10^{-3}$ J m^{-2} from the equilibrated grain boundary groove shapes with a numerical model. The grain boundary energy of the solid Mg_2Zn_{11} phase has been calculated to be $(40.9 \pm 4.5) \times 10^{-3}$ J m^{-2} by considering a force balance at the grain boundary grooves. The thermal conductivity ratio of the eutectic Zn–Mg liquid phase to the solid Mg_2Zn_{11} phase has also been found to be 0.81.

1. Introduction

The solid–liquid interfacial energy, σ_{SL}, is the reversible work required to form or to extend a unit area of interface between a crystal and its coexisting liquid at constant temperature, volume and chemical potential and plays a central role in determining the nucleation rate and growth morphology of the crystal [1–4]. Thus, a quantitative knowledge of σ_{SL} values is necessary. The measurement of σ_{SL} in pure materials and alloys is difficult. Over the last half-century, various attempts have been made to determine the mean value of the solid–liquid interfacial free energy in a variety of materials [1–30]. One of the common techniques for measuring the solid–liquid interfacial free energy is the method of grain boundary grooving in a temperature gradient. In this technique, the solid–liquid interface is equilibrated with a grain boundary in a temperature gradient as shown in figure 1, and the mean value of solid–liquid interfacial free energy is obtained from measurements of the equilibrium shape of the groove profile. The grain boundary groove method is the most useful and powerful technique at present available for measuring the solid–liquid interface energy and can be applied to measure σ_{SL} for multi-component systems as well as pure materials, for opaque materials as well as transparent materials, for any observed grain boundary groove shape and for any $R = K_L/K_S$ value. Over

[3] Author to whom any correspondence should be addressed.

0953-8984/07/176003+14$30.00

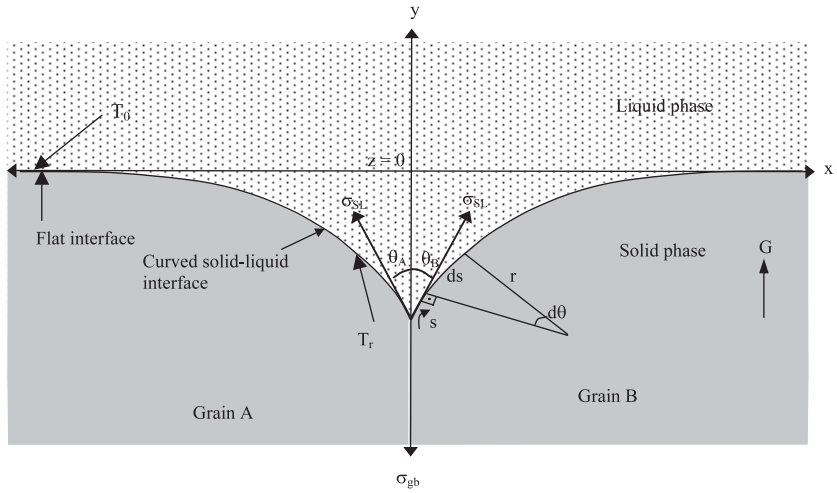

Figure 1. Schematic illustration of an equilibrated grain boundary groove formed at a solid–liquid interface in a temperature gradient showing the x, y coordinates and angle θ.

last 25 years, the equilibrated grain boundary groove shapes in a variety of materials have been observed and measurements of the solid–liquid interfacial free energies made from the observed grain boundary groove shapes [7–30].

In order for a transformation to occur going from the liquid state to the solid state, a material must be held at a temperature T_I which is below the melting temperature, T_m. The system is then said to be undercooled by an amount $\Delta T = T_\mathrm{m} - T_\mathrm{I}$. The transformation from liquid to solid does not occur at the melting temperature, T_m. In a binary alloy, the value of T_I is dependent on the interface curvature, the composition of the liquid and the energy barrier to atoms going from liquid to solid. The undercooling, ΔT, can be given by [31]

$$\Delta T = \Delta T_\mathrm{s} + \Delta T_\mathrm{k} + \Delta T_\mathrm{r} \tag{1}$$

where ΔT_s is the solute undercooling, ΔT_k is the kinetic undercooling and ΔT_r is the curvature undercooling.

In all materials there is an energy barrier to the transfer of atoms from the solid to the liquid phase and vice versa. The solid grows if there is a net transfer of atoms from the liquid to the solid, and this occurs only if the interface is cooled below its melting temperature. This undercooling is called the *kinetic undercooling*, ΔT_k. The liquid phase grows (melting occurs) if there is a net transfer of atoms from the solid to the liquid phase. If the net transfer of atoms is zero, the system is then said to be at equilibrium. The kinetic undercooling, ΔT_k, will be zero at the equilibrium condition for both a one-component system and multi-component systems.

The *solute undercooling*, ΔT_s, is the due to the difference in the liquid composition at the interface and a reference temperature. When the solid–liquid interface is equilibrated with a grain boundary in a temperature gradient, the shape of a grain boundary groove is formed by the intersection of planar grain boundaries with an otherwise planar solid–liquid interface as shown in figure 1. At the equilibrium conditions, the value of ΔT_s will be zero because the composition gradient at the interface is zero.

Thus the total undercooling for a curved interface as shown in figure 1 is equal to the curvature undercooling, i.e. $\Delta T = \Delta T_\mathrm{r}$ at equilibrium conditions. The *curvature undercooling*, ΔT_r, is the temperature difference between the temperature of the flat interface (T_0) and the temperature of the curved interface (T_r). The Gibbs–Thomson undercooling is given by the

following equation for the anisotropic interfacial energy [4]:

$$\Delta T_{\mathrm{r}} = \left[\frac{1}{\Delta S_{\mathrm{f}}}\right]\left[\left(\sigma_{\mathrm{SL}} + \frac{\mathrm{d}^2\sigma_{\mathrm{SL}}}{\mathrm{d}n_1^2}\right)\kappa_1 + \left(\sigma_{\mathrm{SL}} + \frac{\mathrm{d}^2\sigma_{\mathrm{SL}}}{\mathrm{d}n_2^2}\right)\kappa_2\right] \tag{2}$$

where ΔS_{f} is the entropy of fusion per unit volume, $n = (n_x, n_y, n_z)$ is the interface normal, κ_1 and κ_2 are the principal curvatures, and the derivatives are taken along the directions of principal curvature. Thus, the curvature undercooling, ΔT_{r}, is a function of curvature, interfacial free energy and the second derivative of the interfacial free energy. Equation (2) is valid only if the interfacial free energy per unit area is equal to surface tension per unit length, $\sigma_{\mathrm{SL}} = \gamma$ [4]. When the interfacial energy differs from surface tension, the problem is more complicated and the precise modification of the Gibbs–Thomson equation is not yet established [4]. When the solid–liquid interfacial free energy is isotropic, equation (2) becomes

$$\Delta T_{\mathrm{r}} = \frac{\sigma_{\mathrm{SL}}}{\Delta S_{\mathrm{f}}}\left(\frac{1}{r_1} + \frac{1}{r_2}\right) \tag{3}$$

where r_1 and r_2 are the principal radii of curvature. For the case of a planar grain boundary intersecting a planar solid–liquid interface, $r_2 = \infty$ and the equation (3) becomes

$$\Gamma = r\Delta T_{\mathrm{r}} = \frac{\sigma_{\mathrm{SL}}}{\Delta S_{\mathrm{f}}} \tag{4}$$

where Γ is the Gibbs–Thomson coefficient and r is the radius of the groove profile as shown in figure 1. This equation is called the Gibbs–Thomson equation for a curved interface having an isotropic solid–liquid interfacial energy and is useful for considering the effect of solid–liquid interfacial energy on solidification and melting as it expresses the effective change in melting point for a curved interface. At present the most powerful method for measuring solid–liquid interfacial energy experimentally uses the Gibbs–Thomson equation. Equation (4) may be integrated in the y direction (perpendicular to the macroscopic interface from the flat interface to a point on the cusp):

$$\int_0^y \Delta T_{\mathrm{r}}\,\mathrm{d}y = \Gamma\int_0^y \frac{1}{r}\,\mathrm{d}y. \tag{5}$$

The right-hand side of equation (5) may be evaluated for any shape by defining $\mathrm{d}s = r\mathrm{d}\theta$ (s is the distance along the interface and θ is the angle of the interface to y as shown in figure 1) giving

$$\int_0^y \frac{1}{r}\,\mathrm{d}y = (1 - \sin\theta). \tag{6}$$

The left-hand side of equation (5) may be evaluated if ΔT_{r} is known as a function of y.

The left-hand side of equation (5) was integrated numerically using the values of ΔT_{r} calculated numerically and the right-hand side of equation (5) was evaluated by measuring the value of θ (obtained by fitting a Taylor expansion to the adjacent points on the cusp) by Gündüz and Hunt [15, 16]. This allows the Gibbs–Thomson coefficient to be determined for a measured grain boundary groove shape. This numerical method calculates the temperature along the interface of a measured grain boundary groove shape rather than attempting to predict the equilibrium grain boundary groove shape. The shape of the interface, the temperature gradient in the solid, G_{S}, and the ratio of thermal conductivity of the liquid phase to solid phase, $R = K_{\mathrm{L}}/K_{\mathrm{S}}$, must be known or measured to get accurate values for the Gibbs–Thomson coefficient with the Gündüz and Hunt numerical method [15].

No previous attempt has been made to measure the solid–liquid interfacial energy of the solid Mg_2Zn_{11} phase from the observed grain boundary groove shapes in the Zn–Mg system. Therefore the aim of the present work is to determine the Gibbs–Thomson coefficient, solid–liquid interfacial energy and grain boundary energy of the solid Mg_2Zn_{11} phase in equilibrium with Zn–Mg eutectic liquid from the observed grain boundary groove shapes.

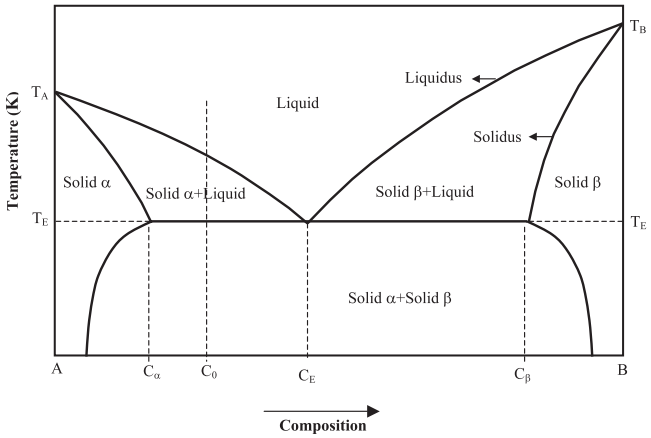

Figure 2. A binary eutectic equilibrium phase diagram.

2. Experimental procedure

2.1. Sample production

The equilibrated solid Mg_2Zn_{11} phase in equilibrium with Zn–Mg eutectic liquid has been observed from the quenched samples by a radial heat flow apparatus originally designed by Gündüz and Hunt [15, 16]. The details of the apparatus and experimental procedures are given in [15–17].

Consider a binary eutectic system as shown in figure 2. Above the eutectic temperature, a binary eutectic system consists of solid and liquid provided the alloy composition, $C_\alpha < C_0 < C_E$ or $C_E > C_0 < C_\beta$, where C_E, C_α and C_β are the composition of the eutectic, solid α and solid β phases, respectively. If this eutectic system is held in a very stable temperature gradient, the liquid droplets move up the temperature gradient by temperature gradient zone melting (TGZM) and a single solid can grow on the eutectic structure during the annealing period. When the composition of alloy is far from the eutectic composition, the experiment usually needs a long time to reach equilibrium due to a larger freezing range. If the alloy composition is near the eutectic composition, above the eutectic temperature, a binary eutectic system consists of liquid. If this system is held in a very stable temperature gradient there will be no liquid droplets behind the solid phase and two solid phases can grow together on the eutectic structure. The equilibration time for this system should be shorter because of the small freezing range.

In the present work the composition of alloys was chosen to be Zn–8 at.% Mg to grow the single solid Zn and Zn_2Mg_{11} phases from the eutectic liquid on the eutectic structures. Zn–8 at.% Mg alloy was prepared in a vacuum furnace by using 99.99% pure zinc and 99.9% pure magnesium. After stirring, the molten alloy was poured into a graphite crucible held in a specially constructed casting furnace at approximately 50 K above the melting point of alloy. The molten metal was then directionally frozen from bottom to top to ensure that the crucible was completely full. The sample was then placed in the radial heat flow apparatus.

The experiments were carried out in two steps. In the first step the thermocouples were calibrated by detecting the melting point during very slow heating and cooling using the lower temperature gradient operational mode. In the second step, the specimen was heated from the centre using a single heating wire (1.7 mm in diameter, Kanthal A-1) and the outside

of the specimen was kept cool with a water cooling jacket. A thin liquid layer (1–2 mm thick) was melted around the central heater and the specimen was annealed in a very stable temperature gradient for a long time. The annealing time for the Zn–8 at.% Mg alloy was 7 days. During the annealing period, the temperature in the specimen and the vertical temperature variations on the sample were continuously recorded by the stationary thermocouples and a moveable thermocouple, respectively, and the input power was recorded periodically. During the experiment, the specimen was kept in a slightly positive pressure of argon to prevent graphite erosion. The temperature in the sample was stable to about ± 0.025 K for hours and ± 0.05 K for up to 7 days. At the end of the annealing time the specimen was rapidly quenched by turning off the input power which is sufficient to get a well defined solid–liquid interface, because the liquid layer around the central heating wire was very thin (typically less than 0.5–1 mm).

2.2. Measurements of the coordinates of equilibrated grain boundary groove shapes

The quenched sample was cut transversely into lengths of typically 25 mm and transverse sections were ground flat with 180-grit SiC paper. Grinding and polishing were then carried out by following the standard route. After polishing, the samples were etched with a 0.4 g $NaSO_4$ and 5 g CrO_3 in 100 ml water enchant for 2 s.

The equilibrated grain boundary groove shapes were then photographed with a CCD digital camera placed in conjunction with an Olympus BH2 light optical microscope using a 20× objective. A graticule ($200 \times 0.01 = 2$ mm) was also photographed using the same objective. The photographs of the equilibrated grain boundary groove shapes and the graticule were superimposed on one another using Adobe PhotoShop version 8.0 software so that accurate measurement of the groove coordinate points on the groove shapes could be made.

2.3. Geometrical correction for the groove coordinates

The coordinates of the cusp, x, y should be measured using the coordinates x, y, z where the x axis is parallel to the solid–liquid interface, the y axis is normal to the solid–liquid interface and the z axis lies at the base of the grain boundary groove as shown in figure 3(a). The coordinates of the cusp x', y' from the metallographic section must be transformed to the x, y coordinates. Maraşlı and Hunt [17] devised a geometrical method to make appropriate corrections to the groove shapes and details of the geometrical method are given in [17].

The relation between x and x' can be expressed as [17]

$$\begin{aligned} x &= x' \cos\alpha \\ x &= x' \frac{\sqrt{a^2 + d^2}}{\sqrt{a^2 + b^2 + d^2}} \end{aligned} \tag{7}$$

and the relation between y and y' can be expressed as [17]

$$\begin{aligned} y &= y' \cos\beta \\ y &= y' \frac{d}{\sqrt{a^2 + d^2}} \end{aligned} \tag{8}$$

where d is the distance between the first and second plane along the z' axis, b is the displacement of the grain boundary position along the x' axis, a is the displacement of the solid–liquid interface along the y' axis, α is the angle between the x' axis and the x axis, and β is the angle between the y' axis and the y axis as shown in figure 3. In this work, the values of a, b and d were measured in order to transform the cusp coordinates x', y' into the x, y coordinates as follows.

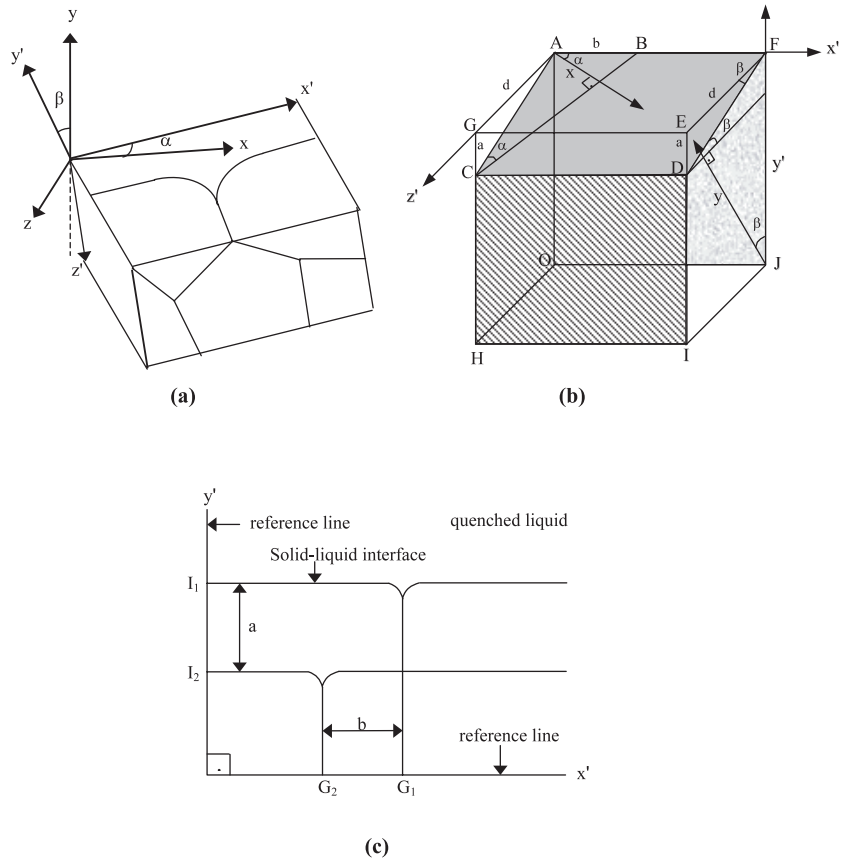

Figure 3. (a) Schematic illustration of the relationship between the actual coordinates, x, y, and the measured coordinates, x', y', of the groove shape. (b) Schematic illustration for the metallic examination of the sample where B is the location of the grain boundary groove shape onto first plane OJFA, C is the location of the grain boundary groove shape onto second plane HIDC, AB $= b$, CG $=$ ED $= a$ and AG $= d$. (c) Schematic illustration of the displacement of the grain boundary groove shape position along the x' and y' axis [17].

Two perpendicular reference lines (≈0.1 mm thick and 0.1 mm deep) were marked near the grain boundary groove on the polished surface of sample (figure 3(c)). The samples were then polished and the grain boundary groove shapes were photographed. The thickness of the sample d_1 was measured with a digital micrometer (with resolution 1 μm) at several points of the sample to obtain the average value. After thickness measurements had been made the sample was again polished to remove a thin layer (at least 40–50 μm) from the sample surface. The same grain boundary groove shapes were again photographed and the thickness of the sample d_2 was measured with the same micrometer. The difference between these sample thicknesses, $d = d_1 - d_2$, gave the layer removed from the sample surface. The photographs of the grain boundary groove shapes were superimposed on one another using Adobe PhotoShop version 8.0 software to measure the displacement of the solid–liquid interface along the y' axis and the displacement of the grain boundary groove position along the x' axis (see figure 3(b)). Thus the required a, b and d measurements were made so that appropriate corrections to the shape of the grooves could be deduced [17].

The coordinates of the equilibrated grain boundary groove shapes were measured with an optical microscope to an accuracy of ± 10 μm. The thickness of the sample (2–2.5 cm lengths) for geometrical correction was measured with a digital micrometer which has ± 1 μm resolution. Thus the uncertainty in the measurements of equilibrated grain boundary coordinates was less than 0.2%.

2.4. Thermal conductivities of the solid and liquid phases

The thermal conductivity ratio of the eutectic liquid phase (Zn–7.8 at.% Mg) to the solid Mg_2Zn_{11} phase (Zn–15.4 at.% Mg alloy), $R = K_{\mathrm{L(eutectic\ liquid)}}/K_{\mathrm{S(solid\ intermetallic)}}$ must be known or measured to evaluate the Gibbs–Thomson coefficients with the present numerical method. The radial heat flow apparatus is an ideal technique for measuring the thermal conductivity of the solid phases.

From Fourier's law, the thermal conductivity of the solid phases at the steady-state conditions can be expressed as

$$K_{\mathrm{S}} = \frac{1}{2\pi\ell} \ln\left(\frac{r_2}{r_1}\right) \frac{Q}{T_1 - T_2} \tag{9}$$

where r_1 and r_2 are fixed distances from the centre of the sample and T_1 and T_2 are the temperatures at the fixed positions r_1 and r_2.

Equation (9) could be used to give the conductivity by measuring the difference in temperature between the two fixed points for a given power level. The difficulty with this is that the error in the calibration of the two thermocouples is likely to be as large as the difference in temperatures. The problem was overcome by measuring the difference in the temperatures for two different power levels and increasing the distance between two thermocouples to 15 mm.

For two different power levels, Q_1 and Q_2, equation (9) can be written as

$$K_{\mathrm{S}} = \frac{1}{2\pi\ell} \ln\left(\frac{r_2}{r_1}\right) \frac{\Delta Q}{\Delta T_1 - \Delta T_2} \tag{10}$$

where ΔQ is the difference in input power and ΔT_1 and ΔT_2 are the temperature differences at r_1 and r_2. This means that the thermal conductivity can be measured accurately even though the absolute temperatures are not known, provided that the vertical temperature variation is minimal or zero.

The thermal conductivities of the solid Mg_2Zn_{11} (Zn–15.4 at.% Mg) and the eutectic solid (Zn–7.8 at.% Mg) were measured in the radial heat flow apparatus. The alloys were prepared in a vacuum furnace by using 99.99% pure zinc and 99.9% pure magnesium. The sample was heated using the central heating wire in steps of 20 K, from 373.2 K up to 5 K below the eutectic temperature (639.3 K). The samples were kept at steady-state for at least 2 h. At the steady-state condition, the total input power, vertical temperature variations on the sample and the temperatures in the sample were measured. When all desired power and temperature measurements had been completed the sample was left to cool down to room temperature. Also to obtain values of K_{S} as a function of temperature it was assumed that conductivity was constant over the interval between two temperature differences.

The thermal conductivities of the solid phases versus temperature are shown in figure 4. The values of K_{S} for the solid Mg_2Zn_{11} and the eutectic solid at their melting point were obtained to be 140.7 and 138.7 W K^{-1} m^{-1}, respectively, by extrapolating to the eutectic temperature as shown in figure 4. The values of thermal conductivities used in the calculations are given in table 1.

It is not possible to measure the thermal conductivity of the liquid phase with the radial heat flow apparatus since a thick liquid layer (10 mm) is required. A layer of this size would

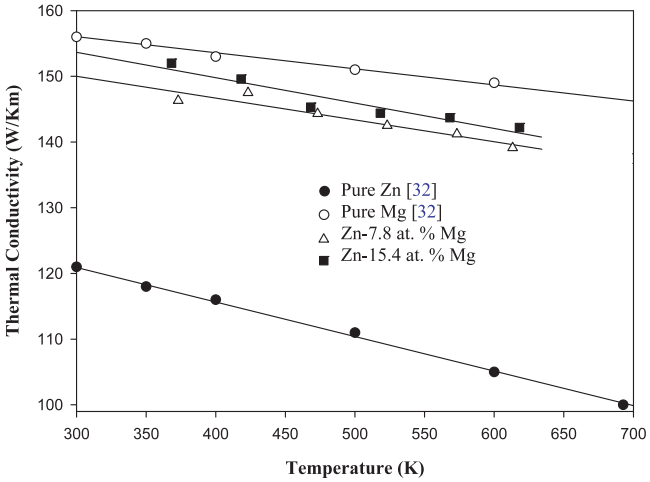

Figure 4. Thermal conductivities of the eutectic solid phase (Zn–7.8 at.% Mg), the solid Mg_2Zn_{11} phase (Zn–15.4 at.% Mg), pure Zn [32] and pure Mg [32].

Table 1. Thermal conductivities of solid and liquid phases and their ratios at the eutectic temperature (639.3 K) for the Zn–7.8 at.% Mg and Zn–15.4 at.% Mg alloys.

System	Phase	Temperature (K)	K (W K^{-1} m^{-1})	$R = K_L/K_S$
Zn–Mg	Liquid (Zn–7.8 at.% Mg)	639.3	113.7	0.82
	Solid (Zn–7.8 at.% Mg)	639.3	138.7	
	Liquid (Zn–7.8 at.% Mg)	639.3	113.7	0.81
	Solid Mg_2Zn_{11} (Zn–15.4 at.% Mg)	639.3	140.7	

certainly have led to convection. If the thermal conductivity ratio of the liquid phase to the solid phase is known and the thermal conductivity of the solid phase is measured at the melting temperature, the thermal conductivity of the liquid phase can then be evaluated. The thermal conductivity ratio can be obtained during directional growth with a Bridgman type growth apparatus. The heat flow away from the interface through the solid phase must balance that in the liquid phase plus the latent heat generated at the interface, i.e. [33]

$$VL = K_S G_S - K_L G_L \tag{11}$$

where V is the growth rate, L is the latent heat, G_S and G_L are the temperature gradients in the solid and liquid, respectively, and K_S and K_L are the thermal conductivities of solid and liquid phases, respectively. For very low velocities, $VL \ll K_S G_S$, so that the conductivity ratio, R is given by

$$R = \frac{K_L}{K_S} = \frac{G_S}{G_L}. \tag{12}$$

A directional growth apparatus, first constructed by McCartney [34], was used to find out the thermal conductivity ratio, $R = K_L/K_S$. A thin walled graphite crucible, 6.3 mm OD × 4 mm ID × 180 mm long, was used to minimize convection in the liquid phase.

Molten Zn–7.8 at.% Mg alloy was poured into the thin walled graphite tube and the molten alloy was then directionally frozen from bottom to top to ensure that the crucible was completely full. The specimen was then placed in the directional growth apparatus. The specimen was heated to 50 K over the melting temperature of alloy. The specimen was then left to reach thermal equilibrium for at least 2 h. The temperature in the specimen was measured with an insulated K type thermocouple. In the present work, a 1.0 mm OD × 0.5 mm ID

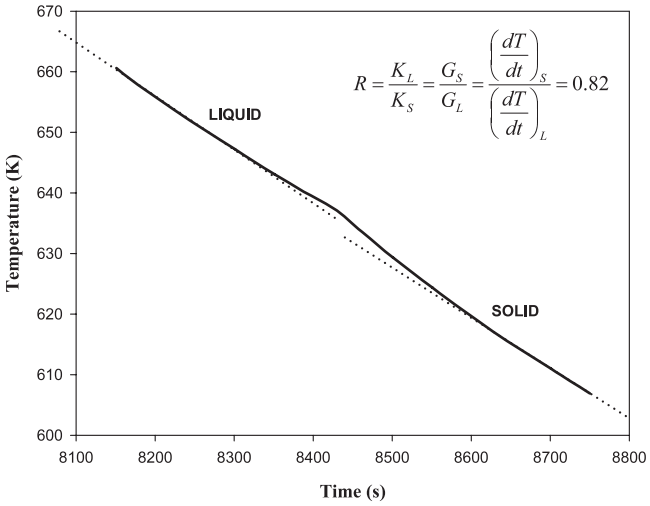

Figure 5. Temperature change versus time for the Zn–7.8 at.% Mg eutectic alloy.

alumina tube was used to insulate the thermocouple from the melts and the thermocouple was placed perpendicular to the heat flow (growth) direction. At the end of equilibration, the temperature in the specimen was stable to ±0.5 K for a short-term period and to ±1 K for a long-term period. When the specimen temperature stabilized, the directional growth was begun by turning the motor on. The cooling rate was recorded with a data logger via a computer. In the present measurements, the growth rate was 8.3×10^{-4} cm s^{-1}. When the solid–liquid interface passed the thermocouple, a change in the slope of the cooling rate for liquid and solid phases was observed. When the thermocouple reading was approximately 30 K below the melting temperature, the growth was stopped by turning the motor off.

The conductivity ratio can be evaluated from the cooling rate ratio of the liquid phase to the solid phase. The cooling rate of the liquid and solid phases is given by

$$\left(\frac{\mathrm{d}T}{\mathrm{d}t}\right)_{\mathrm{L}} = \left(\frac{\mathrm{d}T}{\mathrm{d}x}\right)_{\mathrm{L}}\left(\frac{\mathrm{d}x}{\mathrm{d}t}\right)_{\mathrm{L}} = G_{\mathrm{L}}V \tag{13}$$

and

$$\left(\frac{\mathrm{d}T}{\mathrm{d}t}\right)_{\mathrm{S}} = \left(\frac{\mathrm{d}T}{\mathrm{d}x}\right)_{\mathrm{S}}\left(\frac{\mathrm{d}x}{\mathrm{d}t}\right)_{\mathrm{S}} = G_{\mathrm{S}}V. \tag{14}$$

From equations (12)–(14), the conductivity ratio can be written as

$$R = \frac{K_{\mathrm{L}}}{K_{\mathrm{S}}} = \frac{G_{\mathrm{S}}}{G_{\mathrm{L}}} = \frac{\left(\frac{\mathrm{d}T}{\mathrm{d}t}\right)_{\mathrm{S}}}{\left(\frac{\mathrm{d}T}{\mathrm{d}t}\right)_{\mathrm{L}}} \tag{15}$$

where $(\mathrm{d}T/\mathrm{d}t)_{\mathrm{S}}$ and $(\mathrm{d}T/\mathrm{d}t)_{\mathrm{L}}$ values were directly measured from the temperature versus time curve shown in figure 5. The thermal conductivity ratio of the eutectic liquid phase to the eutectic solid phase, $R_{\mathrm{eutectic}} = K_{\mathrm{L(eutectic)}}/K_{\mathrm{S(eutectic)}}$ was found to be 0.82 as shown in figure 5. The value of $K_{\mathrm{L(eutectic)}}$ was obtained to be 113.7 W K^{-1} m^{-1} by using the values of R_{eutectic} and $K_{\mathrm{S(eutectic)}}$. Thus the thermal conductivity ratio of the eutectic liquid phase to the solid Mg_2Zn_{11} phase, $R = K_{\mathrm{L(eutectic\ liquid)}}/K_{\mathrm{S(solid\ intermetallic)}}$ was obtained to be 0.81 and is also given in table 1.

The estimated experimental error in the measurement of K_{S} is sum of the fractional uncertainty of the measurements of power, temperature difference, length of heating wire and

thermocouple positions which can be expressed as

$$\left|\frac{\Delta K_{\mathrm{s}}}{K_{\mathrm{s}}}\right| = \left|\frac{\Delta(Q_b - Q_a)}{Q_b - Q_a}\right| + \left|\frac{\Delta\left((T_1^b - T_1^a) - (T_2^b - T_2^a)\right)}{(T_1^b - T_1^a) - (T_2^b - T_2^a)}\right| + \left|\frac{\Delta l}{l}\right| + \left|\frac{\Delta r_1}{r_1}\right| + \left|\frac{\Delta r_2}{r_2}\right|. \tag{16}$$

The estimated error in the thermal conductivity measurements is about 5% [35].

2.5. Temperature gradient measurement in the solid phase

The cylindrical sample was heated from the centre by a thin heating wire and a thin liquid layer was melted around the central heating element. The steady-state the temperature gradient at radius r is given by

$$G_{\mathrm{S}} = \frac{\mathrm{d}T}{\mathrm{d}r} = -\frac{Q}{2\pi r \ell K_{\mathrm{S}}} \tag{17}$$

where Q is the input power, ℓ is the length of the heating element, r is the distance of the solid–liquid interface to the centre of the sample and K_{S} is the thermal conductivity of the solid phase.

The average temperature gradient of the solid phase must be determined for each grain boundary groove shape. This was done by measuring the input power, the length of heating element and the position of the solid–liquid interface and the value of K_{S} for the solid Mg_2Zn_{11} phase at the melting point. By using these measured values in equation (17), the temperature gradient can be determined for each grain boundary groove shape.

The estimated experimental error in the measurement of temperature gradient is the sum of the fractional uncertainty of the measurements of power, length of heating wire, thermal conductivity and thermocouple positions which can be expressed as

$$\left|\frac{\Delta G_{\mathrm{S}}}{G_{\mathrm{S}}}\right| = \left|\frac{\Delta Q}{Q}\right| + \left|\frac{\Delta \ell}{\ell}\right| + \left|\frac{\Delta r}{r}\right| + \left|\frac{\Delta K_{\mathrm{S}}}{K_{\mathrm{S}}}\right|. \tag{18}$$

If equation (18) is compared with equation (16), the experimental errors coming from the measurements of Q, ℓ, $r\Delta T$ in equation (18) already exist in the fractional uncertainties in equation (16). Thus the total experimental error in the thermal gradient measurements is equal to the experimental error in thermal conductivity measurements, and is about 5%.

3. Results and discussion

3.1. Determination of the Gibbs–Thomson coefficient

If the thermal conductivity ratio of the liquid phase to the solid phase, the coordinates of the grain boundary groove shapes and the temperature gradient of the solid phase are known, the Gibbs–Thomson coefficient (Γ) can be obtained using the numerical method described in detail [15]. The experimental error in the determination of the Gibbs–Thomson coefficient is the sum of experimental errors in the measurements of the temperature gradient, thermal conductivity and groove coordinates. Thus the total error in the determination of the Gibbs–Thomson coefficient is about 5%.

In the present work, the Gibbs–Thomson coefficients for the solid Mg_2Zn_{11} in equilibrium with Zn–Mg eutectic liquid were determined with the present numerical model by using ten equilibrated grain boundary groove shapes. The grooves examined in this system are shown in figure 6. As can be seen from figure 6, a solid Zn phase (Zn–0.4 at.% Mg) first nucleates on the surface of the solid Mg_2Zn_{11} phase, then both solid Zn and Mg_2Zn_{11} phases grow together to

Table 2. Gibbs–Thomson coefficients for the solid Mg_2Zn_{11} in equilibrium with Zn–Mg eutectic liquid. The subscripts LHS and RHS refer to left-hand side and right-hand side of the grooves, respectively. Note: $\bar{\Gamma} = (3.3 \pm 0.2) \times 10^{-8}$ K m.

				Gibbs–Thomson coefficient	
Groove no	$G_S \times 10^2$ (K m^{-1})	α (deg)	β (deg)	$\Gamma_{LHS} \times 10^{-8}$ (K m)	$\Gamma_{RHS} \times 10^{-8}$ (K m)
a	11.9	14.7	11.4	3.3	3.3
b	12.0	21.3	14.1	3.0	3.4
c	12.4	5.3	26.4	3.1	3.5
d	12.0	2.3	30.2	3.2	3.1
e	12.0	14.0	11.0	3.1	3.0
f	12.1	5.6	16.7	3.3	3.6
g	12.1	20.4	14.7	3.1	3.5
h	12.1	15.8	13.3	3.1	3.7
i	12.2	20.3	27.7	3.3	3.8
j	12.0	15.7	12.0	3.1	3.6

form a eutectic grain. This allows a well defined and fixed solid–liquid interface to be observed during the quench and also the phases, grains and interfaces of the system are very clear. The values of Γ for solid Mg_2Zn_{11} are given in table 2. The average value of Γ from table 2 is $(3.3 \pm 0.2) \times 10^{-8}$ K m for solid Mg_2Zn_{11}.

3.2. Determination of entropy of fusion per unit volume

It is also necessary to know the entropy of fusion per unit volume, ΔS_f, for the solid phase to determine the solid–liquid interfacial energy. For pure materials the entropy of fusion per unit volume is given by

$$\Delta S_f = \frac{\Delta H_M}{T_M} \frac{1}{V_S} \tag{19}$$

where ΔH_M is the enthalpy change of the solid phase at the melting temperature, T_M is the melting temperature and V_S is the molar volume of the solid phase.

The entropy change for an alloy is given by [15],

$$\Delta S_f = \frac{(1 - C_S)(S_A^L - S_A^S) + C_S(S_B^L - S_B^S)}{V_S} \tag{20}$$

where S_A^L, S_A^S, S_B^L and S_B^S are partial molar entropies for materials A and B and C_S is the composition of the solid. Since the entropy terms are generally not available, for convenience the undercooling at constant composition may be related to the change in composition at constant temperature. For a sphere [36]

$$\Delta C_r = \frac{2\sigma_{SL} V_S (1 - C_L) C_L}{r R T_M (C_S - C_L)} \tag{21}$$

where R is the gas constant. For small changes

$$\Delta T_r = m_L \Delta C_r = \frac{2\, m_L \sigma_{SL} V_S (1 - C_L) C_L}{r R T_M (C_S - C_L)}. \tag{22}$$

For a spherical solid $r_1 = r_2 = r$, and from equation (3) the curvature undercooling is written as

$$\Delta T_r = \frac{2\sigma_{SL}}{r \Delta S_f}. \tag{23}$$

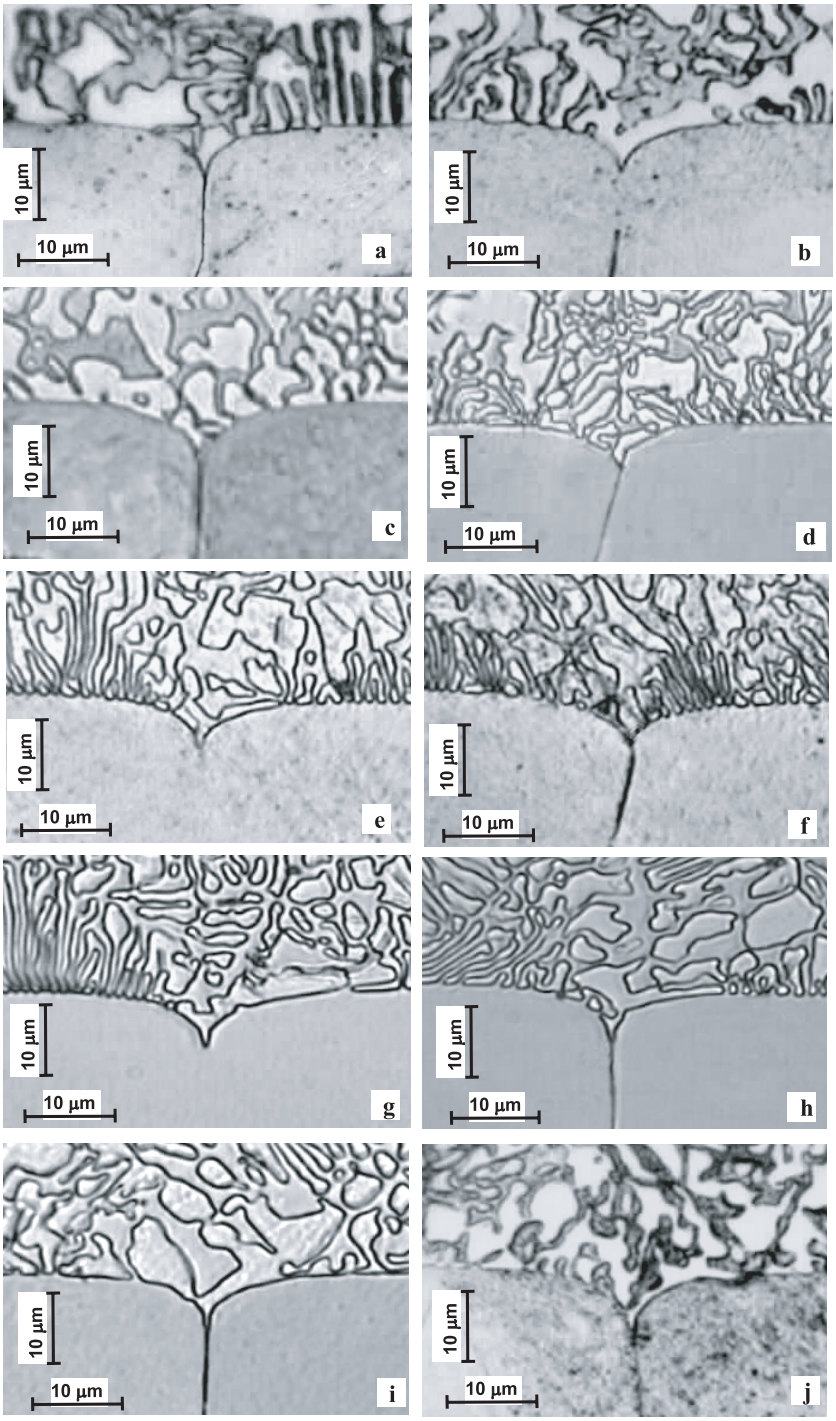

Figure 6. Typical grain boundary groove shapes for the solid Mg_2Zn_{11} in equilibrium with the Zn–Mg eutectic liquid.

Table 3. Some physical properties of the solid Mg_2Zn_{11} phase at the eutectic temperature.

System	Zn–Mg
Composition of the quenched liquid phase, C_L	Zn–7.8 at.% Mg [37]
Composition of solid Mg_2 Zn_{11} phase, C_S	Zn–15.4 at.% Mg [37]
$f(C)$[a]	−1.081
Eutectic melting temperature, T_m (K)	639.28
Molar volume of solid Mg_2Zn_{11}, V_s (m^3)	9.648×10^{-6} [38]
Liquidus slope, m_L (K/ at. fr)	948.62
Entropy change of fusion, ΔS_f (J K^{-1} m^{-3})	6.28×10^5

[a] $f(C) = \frac{C_S - C_L}{(1-C_L)\,C_L}$.

From equations (22) and (23), the entropy change for an alloy is written as

$$\Delta S_f = \frac{RT_M}{m_L V_S} \frac{C_S - C_L}{(1 - C_L)\, C_L}. \tag{24}$$

The values of the relevant constant obtained from [37, 38] and the calculated entropy change of fusion per unit volume are given in table 3. The error in the determined entropy change of fusion per unit volume is estimated to be about 5% [39].

3.3. Evaluation of solid–liquid interfacial energy

If the values of Γ and ΔS_f are known the value of the solid–liquid interfacial energy, σ_{SL}, can be evaluated from equation (3). The solid–liquid interfacial energy of the solid Mg_2Zn_{11} phase in equilibrium with the Zn–Mg eutectic liquid was evaluated to be $(20.8 \pm 2.1) \times 10^{-3}$ J m^{-2} using the values of Γ and ΔS_f. The experimental error in the determined solid–liquid interface energy is the sum of experimental errors of the Gibbs–Thomson coefficient and the entropy change of fusion per unit volume. Thus, the total experimental error for the solid–liquid interfacial energy evaluation in present work is about 10%.

3.4. Grain boundary energy

If the grains on either side of the interface are the same phase then the grain boundary energy can be expressed by

$$\sigma_{gb} = 2\sigma_{SL} \cos\theta \tag{25}$$

where $\theta = \frac{\theta_A + \theta_B}{2}$ is the angle that the solid–liquid interfaces make with the y axis [40]. The angles θ_A and θ_B were obtained from the cusp coordinates, x, y, using a Taylor expansion for parts at the base of the groove. According to equation (25), the value of σ_{gb} should be smaller than or equal to twice the solid–liquid interface energy, i.e. $\sigma_{gb} \leqslant 2\sigma_{SL}$.

The value of the grain boundary energy for the solid Mg_2Zn_{11} phase was found to be $(40.9 \pm 4.5) \times 10^{-3}$ J m^{-2} using the values of σ_{SL} and θ in equation (25). The estimated error in determination of angles θ was found to be 1%. Thus the total experimental error in the resulting grain boundary energy is about 11%.

4. Conclusion

The equilibrated grain boundary groove shapes of the solid Mg_2Zn_{11} phase in equilibrium with the Zn–Mg eutectic liquid have been observed from the quenched samples with a radial heat flow apparatus. From the observed grain boundary groove shapes, the Gibbs–Thomson

coefficient, solid–liquid interfacial energy and the grain boundary energy of the solid Mg_2Zn_{11} phase in equilibrium with the Zn–Mg eutectic liquid have been determined. The thermal conductivity ratio of the equilibrated the Zn–Mg eutectic liquid to the solid Mg_2Zn_{11} phase has also been measured.

Acknowledgments

This study was supported by the Erciyes University Scientific Research Project Unit under contract no. FBT-04-19. The authors are grateful to Erciyes University Scientific Research Project Unit for their financial support.

References

[1] Turnbull D 1950 *J. Appl. Phys.* **21** 1022
[2] Jones D R H 1974 *J. Mater. Sci.* **9** 1
[3] Jackson C L and McKenna G B 1990 *J. Chem. Phys.* **93** 9002
[4] Trivedi R and Hunt J D 1993 *The Mechanics of Solder Alloy Wetting and Spreading* (New York: Van Nostrand-Reinhold) p 191
[5] Morris J R and Napolitano R E 2004 *JOM* **56** 40
[6] Hoyt J J, Asta M, Haxhimali T, Karma A, Napolitano R E and Trivedi R 2004 *MRS Bull.* **29** 935
[7] Jones D R H and Chadwick G A 1970 *Phil. Mag.* **22** 291
[8] Jones D R H and Chadwick G A 1971 *J. Cryst. Growth* **11** 260
[9] Jones D R H 1978 *Phil. Mag.* **27** 569
[10] Schaefer R J, Glicksman M E and Ayers J D 1975 *Phil. Mag.* **32** 725
[11] Hardy S C 1977 *Phil. Mag.* **35** 471
[12] Nash G E and Glicksman M E 1971 *Phil. Mag.* **24** 577
[13] Bolling G F and Tiller W A 1960 *J. Appl. Phys.* **31** 1345
[14] Singh N B and Glicksman M E 1989 *J. Cryst. Growth* **98** 573
[15] Gündüz M and Hunt J D 1985 *Acta Metall.* **33** 1651
[16] Gündüz M and Hunt J D 1989 *Acta Metall.* **37** 1839
[17] Maraşlı N and Hunt J D 1996 *Acta Mater.* **44** 1085
[18] Stalder I and Bilgram J H 2003 *J. Chem. Phys.* **118** 798
[19] Bayender B, Maraşlı N, Çadırlı E, Sişman H and Gündüz M 1998 *J. Cryst. Growth* **194** 119
[20] Bayender B, Maraşlı N, Çadırlı E and Gündüz M 1999 *Mater. Sci. Eng.* A **270** 343
[21] Maraşlı N, Keşlioğlu K and Arslan B 2003 *J. Cryst. Growth* **247** 613
[22] Böyük U, Keşlioğlu K, Erol M and Maraşlı N 2005 *Mater. Lett.* **59** 2953
[23] Keşlioğlu K, Böyük U, Erol M and Maraşlı N 2006 *J. Mater. Sci.* **41** 7939
[24] Ocak Y, Akbulut S, Böyük U, Erol M, Keşlioğlu K and Maraşlı N 2006 *Scr. Mater.* **55** 235
[25] Ocak Y, Akbulut S, Böyük U, Erol M, Keşlioğlu K and Maraşlı N 2006 *Thermochim. Acta* **55** 235
[26] Keşlioğlu K and Maraşlı N 2004 *Mater. Sci. Eng.* A **369** 294
[27] Keşlioğlu K and Maraşlı N 2004 *Metall. Mater. Trans.* A **35A** 3665
[28] Erol M, Maraşlı N, Keşlioğlu K and Gündüz M 2004 *Scr. Mater.* **51** 131
[29] Keşlioğlu K, Erol M, Maraşlı N and Gündüz M 2004 *J. Alloys Compounds* **385** 207
[30] Erol M, Keşlioğlu K and Maraşlı N 2007 *Metall. Mater. Trans.* A at press
[31] Burden M H and Hunt J D 1974 *J. Cryst. Growth* **22** 109
[32] Touloukian Y S, Powell R W, Ho C Y and Klemens P G 1970 *Thermal Conductivity Metallic Elements and Alloys* (New York: Plenum) pp 207–460
[33] Porter D A and Easterling K E 1991 *Phase Transformations in Metals and Alloys* (Boca Raton, FL: CRC Press) p 204
[34] McCartney D G 1981 *DPhil Thesis* University of Oxford, UK, p 85
[35] Erol M, Keşlioğlu K, Şahingöz R and Maraşlı N 2005 *Met. Mater. Int.* **11** 421
[36] Christian J W 1975 *The Theory of Transformations in Metals and Alloys* 2nd edn (Oxford: Pergamon) part I p 169
[37] Massalski T B, Okamoto H, Subramanian P R and Kacprzak L 1990 *Binary Alloy Phase Diagrams* (Metals Park, OH: ASM International) pp 271–777
[38] Suryanarayana C and Norton M G 1998 *X-Ray Diffraction—A Practical Approach* (New York: Plenum) p 263
[39] Tassa M and Hunt J D 1976 *J. Cryst. Growth* **34** 38
[40] Woodruff P 1973 *The Solid–Liquid Interface* (Cambridge: Cambridge University Press)